https://doi.org/10.5194/egusphere-2024-733
Preprint. Discussion started: 19 March 2024

Measurement report: In-situ vertical profiles of below-cloud aerosol over the central Greenland Ice Sheet.

Heather Guy[1,2], Andrew S. Martin[1,2], Erik Olson[3], Ian M. Brooks[2], and Ryan R. Neely III[1,2]

[1]National Centre for Atmospheric Science, Leeds, U.K.
[2]School of Earth and Environment, University of Leeds, Leeds, U.K.
[3]Space Science and Engineering Center, UW-Madison, Madison, WI, USA

Correspondence: Heather Guy (heather.guy@ncas.ac.uk)

Abstract.

Surface radiative cooling in polar regions can generate persistent stability in the atmospheric boundary layer. Stable layers below clouds can decouple the cloud layer from the near-surface environment. Under these conditions, surface aerosol measurements are not necessarily representative of the near-cloud or intra-cloud aerosol populations. To better understand the variability in the vertical structure of aerosol properties over the central Greenland Ice Sheet, in-situ measurements of aerosol particle size distributions up to cloud base were made at Summit Station in July and August 2023. These measurements identified distinct vertical aerosol layers between the surface and cloud base associated thermodynamic decoupling layers. Such decoupling layers occur 49% of the time during the summer in central Greenland, suggesting that surface aerosol measurements are insufficient to describe the cloud-relevant aerosol population half of the time. Experience during this first measurement season demonstrated the ability of a tethered balloon platform to operate effectively under icing conditions and at low surface pressure ($<$ 680 hPa). The results presented here illustrate the value of vertically resolved in-situ measurements of aerosol properties to develop a nuanced understanding of the aerosol effects on cloud properties in polar regions.

1 Introduction

Clouds are an important control on the surface energy budget of the Greenland Ice Sheet (GrIS). Clouds increase downwelling longwave radiation relative to equivalent clear sky conditions and, in the summer, they shade the surface from incoming solar radiation. The net radiative effect of clouds at the surface depends on the incoming solar radiation and surface albedo as well as the temperature, optical depth, and microphysical properties of the cloud (Shupe and Intrieri, 2004). As a result, changes in cloud cover over the GrIS can have either a net warming or a net cooling effect at the surface, which is both regionally and seasonally dependent. Van Tricht et al. (2016) demonstrated that, on annual timescales, the longwave warming effect of clouds prevails, leading to an overall warming of the ice sheet. Conversely, Hofer et al. (2017) found that a reduction in summer cloud cover enhances net downwelling radiation over the lower albedo ablation zone, resulting in increased surface melt. Cloud radiative forcing is particularly sensitive to the integrated amount of cloud liquid water (liquid water path, LWP, e.g. Miller et al., 2015). Bennartz et al. (2013) showed that LWP was a critical control on surface melt in central Greenland during the

https://doi.org/10.5194/egusphere-2024-733
Preprint. Discussion started: 19 March 2024

extreme melt event in July 2012. Understanding the processes that control LWP and cloud lifetime over the GrIS is essential for understanding how the GrIS surface energy budget will respond to changes in cloud cover.

Aerosol particles are an important control on cloud lifetime and phase, and hence LWP. The abundance of ice nucleating particles (INPs) in a supercooled cloud can determine how much ice forms. When the air is supersaturated with respect to ice but subsaturated with respect to water, ice particles will grow at the expense of liquid droplets, reducing LWP and longwave cloud radiative forcing (e.g.Korolev, 2007). Since ice particles tend to be larger than liquid droplets, ice formation controlled by the abundance of INPs can impact cloud lifetime (e.g. Storelvmo et al., 2011). The abundance of particles that can nucleate liquid cloud droplets (cloud condensation nuclei, CCN), controls the number of cloud droplets that form at a given supersaturation. This means that a cloud with the same liquid water content, but fewer CCN, will consist of fewer, larger cloud droplets (Twomey, 1977). Such a cloud would be less opaque than the equivalent cloud with more CCN, increasing shortwave transmittance. In extreme cases, a lack of CCN can trigger a positive feedback where the few activated droplets grow large enough to precipitate out, removing any remaining CCN and limiting cloud LWP, longwave emissivity, and cloud lifetime (Mauritsen et al., 2011; Sterzinger et al., 2022).

Despite the potential sensitivity of cloud properties, and therefore cloud radiative forcing, to the number concentrations of CCN and INP, measurements of aerosol properties over the GrIS are sparse (Schmale et al., 2021). Year-round surface-based measurements of particle number concentrations and size distributions, which are important for determining the concentrations of CCN and INP, are only available from Villum Research Station (north-east Greenland) since 2010 and from Summit Station (central GrIS) since 2019 (fig. 1). Villum, like other coastal Arctic sites, is sensitive to Arctic haze and marine aerosol sources (Nguyen et al., 2016; Freud et al., 2017; Lange et al., 2018), whereas Summit is sensitive to the descent of aerosol particles from the free troposphere (Hirdman et al., 2010; Law et al., 2014; Guy et al., 2021). Since the primary source of aerosol particles at Summit is descent from above, surface measurements are strongly impacted by fog scavenging and air mass isolation below near-surface temperature inversions, implying that they might not be representative of the aerosol population higher in the atmosphere (Dibb et al., 1992; Bergin et al., 1994, 1995; Guy et al., 2021, 2023).

Near-surface temperature inversions, formed by radiative cooling of high emissivity snow- and ice-covered surfaces in the Arctic, can act to thermodynamically decouple the surface from the upper boundary layer, even in the presence of low-level cloud (Shupe et al., 2013; Sotiropoulou et al., 2014; Brooks et al., 2017). Where such decoupling occurs, distinct differences between the surface and cloud-relevant aerosol populations have been directly observed (Igel et al., 2017; Creamean et al., 2021; Lonardi et al., 2022; Zhang et al., 2022). Creamean et al. (2021) use equivalent potential temperature profiles (a measure of static stability), alongside vertically resolved measurements of particle number concentrations from Oliktok Point in Alaska, to show that whether or not the surface aerosol population is similar to that at cloud base is tightly coupled to the thermodynamic mixing state of the boundary layer.

Over central Greenland, near-surface temperature inversions occur over 70% of the time (Hoch et al., 2007; Miller et al., 2013), and the high static stability within the inversion inhibits vertical mixing. Despite the importance of understanding the cloud-relevant aerosol population over the GrIS, and the fact that this population is likely to differ from that at the surface due to the high near-surface static stability, measurements of aerosol particles at cloud height over the GrIS are limited to

https://doi.org/10.5194/egusphere-2024-733
Preprint. Discussion started: 19 March 2024

just a handful of aircraft campaigns (Flyger et al., 1973, 1976; Law et al., 2014). Although useful for understanding aerosol properties at cloud height, the spatial and temporal resolution of aircraft measurements are severely limited, and aircraft are unable to take repeated measurements close to the surface to understand the relationship between surface aerosol properties, which are relatively straightforward to measure, and those at cloud height.

Here we demonstrate the use of a tethered balloon platform to measure vertically resolved aerosol particle size distributions up to 830 m a.g.l over the central GrIS. Although limited to just six opportunistic sampling days in July and August of 2023, the measurements demonstrate the utility of this measurement platform in the cold, remote, and high-altitude environment of central Greenland, paving the way for future campaigns of longer duration that are necessary to understand the vertical structure of near-surface aerosol particles over the GrIS, and their relevance for radiatively important cloud properties.

2 Measurements

2.1 Sampling location

Summit Station (72.58°N, -38.45°E) is in the accumulation zone of the GrIS, on the summit plateau 3,250 m above mean sea level (fig. 1). There are no local sources of primary aerosol particles apart from station emissions. As an atmospheric baseline sampling site, non-essential emissions are strictly controlled to protect the quality of long-term trace gas measurements collected in a 'clean air zone' south of the main station. The base station for vertical aerosol profiling was ∼2,600 m west of the main station generator (fig. 1). Measurement contamination by pollution from the main station generator may have occurred on 04 August during persistently low winds, this is discussed further in section 3.

The measurement platform was attached to a 1 km tether that was passed through an anchored redirection point at the base station. The other end of the tether was attached to a snowmobile which was used to raise and lower the measurement platform. As part of the station-wide emission control protocol, we were not permitted to operate the snowmobile in wind directions between 285° and 39°. Unfortunately, 10 of 14 possible sampling days were impacted by this restriction, which significantly limited the number of profiles we were able to sample during this campaign.

2.2 Instrumentation and measurement platform

Vertical profiling was enabled by a 21 m^3 Helikite (fig. 2). The Helikite is a tethered helium filled balloon with a kite wing that provides orientation, stabilisation, and additional dynamic lift (Allsopp Helikites Ltd., 2023). At sea level pressure, the balloon envelope provides 12 kg of static lift. At Summit Station, where the mean surface air pressure in summer is 680 hPa, the static lift is reduced to 5 kg. In winds of 4.2 m s^{-1}, the kite wing increases the lift by ∼50%, according to the manufacturer. A 1 km tether (2.5 mm diameter line weighing 4.9 g m^{-1}) was selected to provide the maximum sampling altitude whilst allowing sufficient lift for the instrument package at full tether extension. The main advantages of the Helikite platform over drone or aircraft platforms are that it can sample through clouds, in icing conditions, and can profile in the same location for extended periods of time. Ice forming on the Helikite and tether may cause the Helikite to descend gradually, but not result in a

https://doi.org/10.5194/egusphere-2024-733
Preprint. Discussion started: 19 March 2024

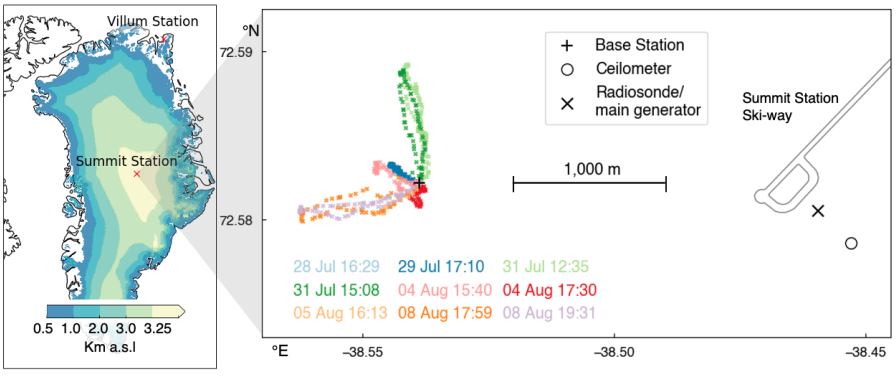

Figure 1. Location and map of Summit Station. Coloured makers show the location of the measurement package during sampling with relation to the tethered balloon base station on the ground, which is also indicative of the wind direction during each profile. Ice elevation contours are from the Greenland Ice Mapping Project (Howat et al., 2017).

Figure 2. Inflated Helikite and instrument payload.

sudden uncontrolled loss of altitude. The Helikite can nominally operate in wind speeds of 0 to 18 m s^{-1}, although in practice, managing the Helikite on the surface was challenging when winds exceeded 7 m s^{-1}.

The instrument package consisted of a Handix Portable Optical Particle Spectrometer (POPS, Gao et al., 2016; Mei et al., 2020), and a reusable S1H3 Windsond radiosonde. The POPS measured size-resolved aerosol particle number concentrations in 16 bins (115 and 3370 nm diameter) with a flow rate of 3 cm^3 s^{-1}. The instrument electronics were placed in a lightweight insulating foam box, and a coarse mesh filter was placed over the inlet to prevent the growth of rime ice on the inlet itself. The POPS was secured to the kite wing such that the inlet was always oriented into the wind (fig. 2). The radiosonde included an integrated GPS unit and measured air pressure, temperature, and relative humidity at 1 Hz with accuracies of ± 1 hPa, 0.3 °C, and 2% respectively. Radiosonde data were transmitted in real-time to the base station. The combined instrument payload of the POPS, radiosonde, and battery pack weighed 3 kg.

https://doi.org/10.5194/egusphere-2024-733
Preprint. Discussion started: 19 March 2024

Post-processing of the radiosonde data revealed unrealistic temperature increases when the measurement platform was stationary or moving slowly, presumably associated with insufficient ventilation of the sensor. To correct for this, we applied the following four-stage quality control procedure to the radiosonde data:

1. Removal of measurements collected when the measurement platform was moving slower than 0.5 m s^{-1}.
2. Application of a despiking algorithm to remove data points when the sensor was re-equilibrating. This algorithm identifies and removes points that lie outside of one standard deviation from the 50 m rolling mean of the temperature profile. This is repeated three times.
3. Manual removal of any remaining suspect data points. This included the lowest 30 m for all profiles where it was unclear if the sensor was equilibrated with ambient conditions after being stationary at the surface.
4. Linear interpolation of the remaining data and calculation of a 20 m rolling mean.

The resulting temperature and humidity profiles were similar to those output by the Windsond automated algorithm (which calculates 20 m averages during ascent), but additionally include data from the descending profiles.

2.3 Case studies

Conditions were suitable for operating the tethered balloon on 13 out of 14 potential sampling days from 25 July to 09 August 2023 (on 09 August the wind speed was too high, $>$10 m s^{-1}). Unfortunately, due to restrictions on snowmobile usage under certain wind directions (described in 2.1), we were only able to collect nine vertical profiles over six days (Table 1). We focused on sampling the vertical aerosol profile below cloud base, although sampling through cloud would be possible during future campaigns with appropriate flying permissions. Horizontally extensive low-level stratocumulus or broken altocumulus, with cloud base ranging from 300 to 1,700 m a.g.l, was present on each sampling day. The sampled air pressure ranged from 617 to 684 hPa, and air temperature between -13.5 and -3.7 °C. The maximum 10 m wind speed during tethered balloon operations was 6.8 m s^{-1}. The maximum sampling altitude of 830 m a.g.l was achieved at full tether extension on a low wind day (04 August) when there was insufficient lift to fly higher. When wind speeds were faster, the maximum flying altitude was limited by the smaller angle of inclination between the tether and the ground. Repeat profiles were collected on the three days we were able to sample above 500 m a.g.l (31 July, 04, and 08 August).

2.4 Cloud and boundary layer structure

Additional information on the temporal evolution of cloud properties and boundary layer structure during the campaign are available from a Vaisala CT25K ceilometer and twice daily launches of Vaisala RS41 radiosondes (at 00 and 12 UTC) as part of the 'Integrated Characterisation of Energy, Clouds, Atmospheric properties, and Precipitation at Summit' project (ICECAPS, Shupe et al., 2013). The ceilometer measured range and sensitivity normalised backscatter (at 905 nm, see Münkel et al., 2007), and cloud base height. Although there were no direct precipitation measurements during the campaign, precipitation occurrence and timing on sampling days was logged by on-site observers.

https://doi.org/10.5194/egusphere-2024-733
Preprint. Discussion started: 19 March 2024

Table 1. Sampling times and associated atmospheric conditions. Altitude, air pressure, temperature, and relative humidity are from the radiosonde. Wind speed and direction (10 m) during each sampling period are from the NOAA GML meteorological station (NOAA-GML, 2023), and mean cloud base height is from the ICECAPS ceilometer (Shupe, 2010). Sample profiles are organised so that the lower altitude profiles are labelled (a)-(c) and the higher profiles (d)-(f).

ID	Date DD/MM 2023	Sampling time start/end (UTC)	Max profile altitude (m a.g.l)	Air pressure Max/min (hPa)	Air temperature Max/min °C	Relative humidity w.r.t. water Max/min	10 m Wind speed Max/min (m s^{-1})	10 m Wind direction Mean (°)	Cloud base height median (m a.g.l)
(a)	28/07	16:09/18:13	158	682/673	-6.3/-7.4	79/73	6.7/4.3	108	315
(b)	29/07	17:00/19:00	262	678/659	-7.5/-9.9	79/72	5.1/3.4	114	390
(c)	05/08	16:05/17:26	310	684/659	-10.3/-12.4	78/69	3.3/1.8	19	1545
(d)	31/07	12:33/14:39	636	676/622	-7.4/-13.5	73/60	3.1/1.2	198	1080
(d_1)	31/07	15:00/16:30	680	676/622	-7.4/-13.5	77/64	2.4/0.4	205	1050
(e)	04/08	14:35/17:09	824	679/617	-3.7/-11.3	69/35	2.0/0.1	13	1650
(e_1)	04/08	17:25/18:46	830	679/617	-5.0/-11.3	69/35	2.6/0.9	1	1680
(f)	08/08	17:56/19:15	636	684/634	-9.4/-13.4	80/75	6.8/5.2	56	1035
(f_1)	08/08	19:27/20:47	618	684/636	-9.8/-13.2	85/74	6.6/3.8	67	975

To explore how the vertical structure of the aerosol particle size distribution is related to the thermodynamic structure of the boundary layer, profiles of equivalent potential temperature (θ_e) were derived from the Windsond measurements. Averaged vertical particle size distributions and θ_e as a function of height for each profile (ascending and descending combined) were calculated by gridding the data onto regular 5 m vertical intervals and calculating a 20 m rolling mean. Thermodynamically stable 'decoupling layers', across which turbulent mixing is inhibited, were identified where θ_e increased monotonically with height for at least 20 m, following the methodology of Vüllers et al. (2021). Neutral / weakly stable layers were removed by applying the criterion that each decoupling layer must have a minimum 0.1 K increase in θ_e. Individual layers were merged into a single layer if they were separated by less than 100 m vertically.

3 Results

3.1 Vertical aerosol profiles and sky condition

Figure 3 shows the measurement altitude and total particle number concentration (115 to 3370 nm) in relation to the ceilometer backscatter profile for each sampling day. In case (a), the Windsond failed at the highest point in the profile and there were no measurements during the descent. Note that the ceilometer clearly identifies cloud base height, but the signal may be attenuated within the cloud and therefore does not reliably show the cloud vertical extent. The overall range of total aerosol

https://doi.org/10.5194/egusphere-2024-733
Preprint. Discussion started: 19 March 2024

particle number concentrations was 14 to 55 cm^{-3}. We did not sample any days where the total particle number concentration approached < 10 cm^{-3}, which would be potentially indicative of an aerosol-limited cloud regime, although this is known to occur at Summit (Guy et al., 2021).

On the first two sampling days (fig. 3a and b, 28 and 29 July), the cloud base was less than 400 m, and there was little variation in the total particle number concentration with altitude below the cloud. However, on the latter four days, when the cloud base was higher (950 to 1,700 m), altitude-dependent variations in the particle number concentration below cloud base were apparent (fig. 3).

During case (c), we were unable to sample up to cloud base due to the implementation of a station wide restriction on snowmobile usage. Nevertheless, there was a clear difference between the particle number concentration near the surface ($<$ 40 cm^{-3}) and that above 250 m ($>$ 50 cm^{-3}). One hour prior to sampling, a precipitating stratus cloud was present at the approximate height of the increase in particle number concentration (fig. 3c). There was also fog early in the morning that day, which is known to contribute to the wet scavenging of aerosol particles in the surface layer (Guy et al., 2021).

During case (d), it was snowing prior to sampling (between 04 and 10 UTC), from a cloud with a base height of ∼300 m. During sampling, a cloud with base height of 1080 m thinned and began to break up, and observers noted intermittent light snow at the surface. Both profiles on this day showed an increase in particle number concentrations with height from ∼30 cm^{-3} near the surface to $>$ 50 cm^{-3} above 300 m (fig. 3d).

Low wind speeds (0.1 to 2.6 m s^{-1}) during case (e) allowed us to manually raise and lower the tethered balloon without the use of a snowmobile. On this occasion, particle number concentrations were higher close to the surface than aloft. In both repeat profiles, there was a distinct, relatively low particle number concentration layer between 350 and 500 m (fig. 3e). Earlier in the day (between 04 and 12 UTC), it had been snowing heavily from a cloud layer at ∼400 m.

The strong signal in the ceilometer backscatter during case (f) was caused by intermittent snow squalls beneath broken altocumulus cloud. Particle concentrations were relatively low compared to previous days (median value 22 cm^{-3}), but increased with altitude in both profiles (fig. 3f). On each of the three days when a repeat profile was possible, the vertical distribution of aerosol particles was similar between the two repeats (fig. 3d-f). For the rest of the figures in this paper, only the first of the two repeats are shown.

3.2 Relationship to boundary layer structure

On five of the six sampling days, the Windsond θ_e profile indicated that the cloud layer was thermodynamically decoupled from the surface. The mean height of the lower boundary of the decoupling layer was 196 m a.g.l (fig. 4). No θ_e profile is shown for case (a) due to a Windsonde failure resulting in a lack of quality temperature and humidity measurements, however, the particle size distribution was well mixed throughout the profile (up to 130 m, fig. 4a). During case (b), the boundary layer was neutral up to a weakly stable (0.5 K) decoupling layer at 78-150 m. Above the decoupling layer, there were fewer smaller particles ($<$ 250 nm diameter) compared to within the surface layer (fig. 4b, fig. 5b).

During case (c), the near surface layer was well-mixed up to the start of a stable layer at 68 m (fig. 4c). A second, deeper stable layer above a shallow mixed layer at 120 m was not identified as a second decoupling layer since the separation between

https://doi.org/10.5194/egusphere-2024-733
Preprint. Discussion started: 19 March 2024

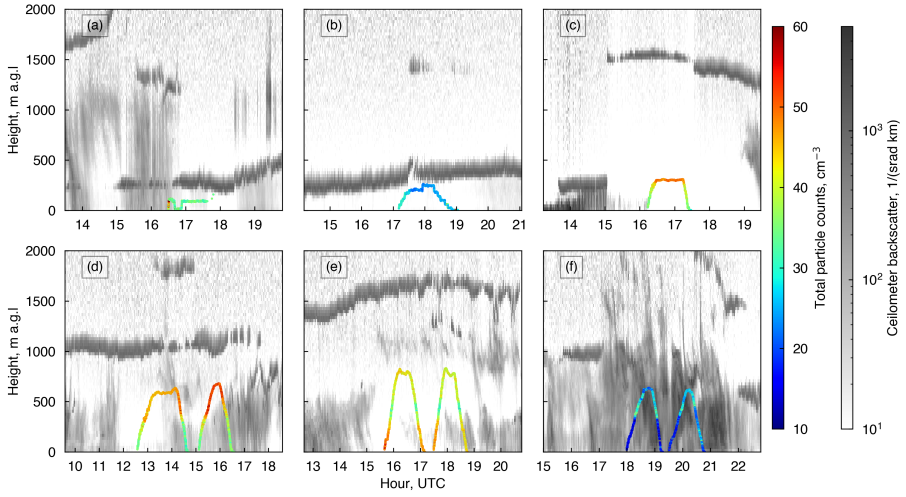

Figure 3. Vertical profiles overlain on ceilometer backscatter and coloured by total particle number concentration.

the two layers was less than 100 m (fig. 4c). On this occasion there was a notable increase in smaller particles ($<$ 300 nm diameter) above the surface mixed layer, with an 22% increase in particles smaller than 200 nm (fig. 5c). Fig. 4c shows that most of the increase in smaller particles occurred above ∼200 m (i.e. 130 m higher than the lower boundary of the stable decoupling layer).

Two decoupling layers were identified for case (d). The first is a weak (0.3 K), shallow stable layer at 123 m, above the well-mixed surface layer, and the second is a stronger inversion (1.22 K) with a base at 398 m (fig. 4d). Particle number concentrations increase with height from ∼200 m up to the base of the second decoupling layer, and this increase is most pronounced for 160 to 400 nm diameter particles (fig. 4d, 5d). Above the second decoupling layer, the particle size distribution is relatively constant with height but distinct from the particle size distribution in the surface mixed layer (fig. 4d, 5d).

The surface layer was mostly well-mixed during case (e) up to a strong (6.3 K) decoupling layer with a base 258 m. Most of the inversion occurs in the first 150 m above that decoupling level, generating the steepest gradient in θ_e of the six cases (fig. 4e). The thermodynamically isolated surface layer had the highest concentrations of 115 to 400 nm particles in the vertical profile of all the six cases (fig. 5e). Since wind speeds on this day were notably slow (the mean wind speed in the 12 hours prior to sampling was 1.8 m s^{-1}), the increased particle number concentrations beneath the lowest decoupling layer could have resulted from a build-up of local pollution around the research station. Above the base of the decoupling layer there was a sharp decrease in particle number concentrations, particularly in the 140 to 280 nm diameter range. In all size bins, the lowest particle number concentrations occurred in a distinct layer between 350 and 500 m. At 500m, just above the strongest part of the decoupling layer, particle number concentrations increased again in all size bins and were then more or less constant with height for the rest of the profile (fig. 4e).

Finally, during case (f), the particle size distribution was constant with height throughout the well-mixed surface layer. At ∼300 m, there was a sharp increase in the number concentration of 115 to 300 nm diameter particles, just above the lower

https://doi.org/10.5194/egusphere-2024-733
Preprint. Discussion started: 19 March 2024

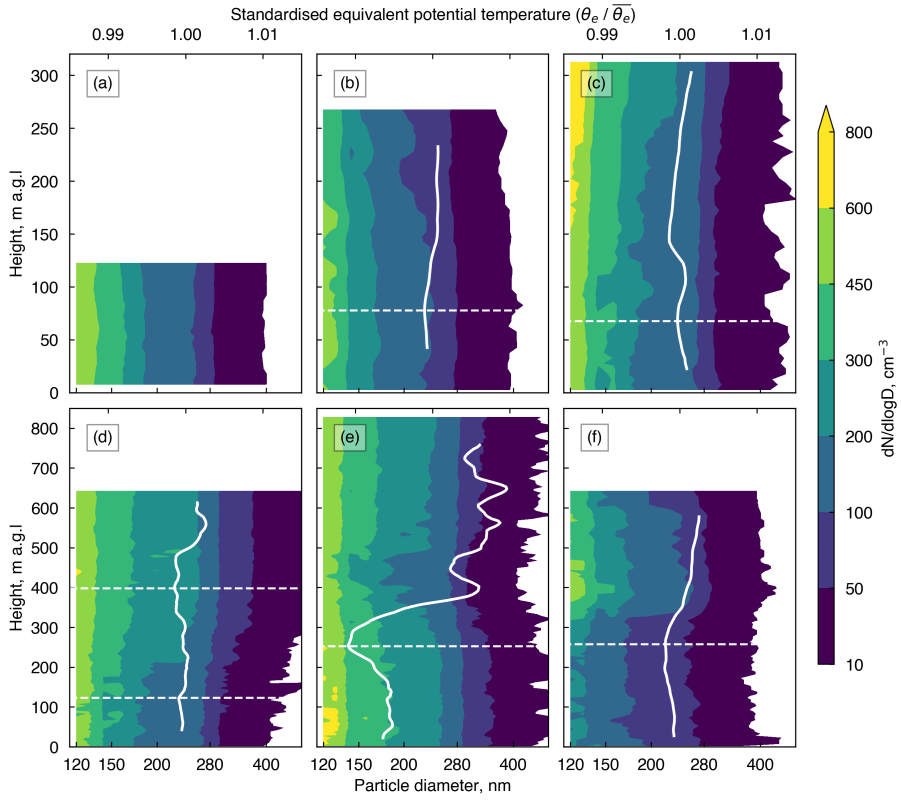

Figure 4. Particle size distributions (20 m rolling mean, contoured) and standardised equivalent potential temperature profiles ($\theta_e/\overline{\theta_e}$, thick white line) for each profile. The three lower altitude flights are on the top row (note the difference in y-axis scales). Horizontal dashed lines indicate the lower boundaries of thermodynamically stable 'decoupling' layers.

boundary of a stable decoupling layer at 258 m (fig. 4f). Above this level the size distribution was approximately constant with height again, resulting in a clear distinction between the particle size distribution in the surface layer and that in the below-cloud environment (fig. 5f).

4 Discussion

In summary, on five out of six sampling days, at least one thermodynamically stable layer was identified which would have inhibited the turbulent mixing of aerosol particles between the near-surface layer and the below-cloud environment (fig 4). On each of those days, the total particle number concentration and size distribution varied as a function of height above the lower boundary of the thermodynamically stable layer (figs. 4 and 5). On the day when there were insufficient measurements to calculate the θ_e profile (case a), the particle number concentration and size distribution was consistent with height up to cloud base, suggesting that this profile was well-mixed.

https://doi.org/10.5194/egusphere-2024-733
Preprint. Discussion started: 19 March 2024

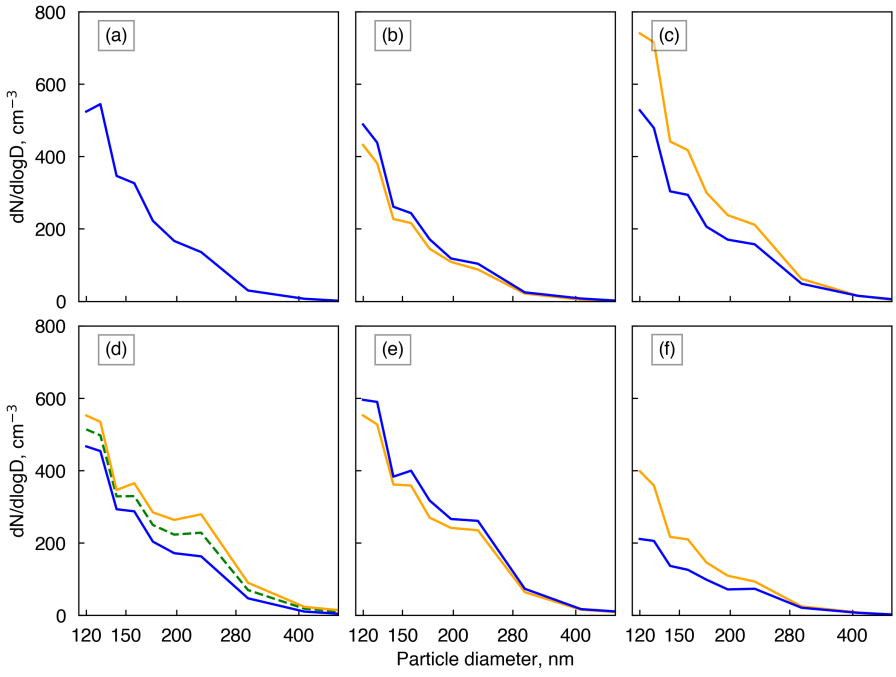

Figure 5. Mean particle size distribution in the surface layer (blue) compared to the highest layer sampled (orange). Where two decoupling heights were identified, the mean size distribution of the layer between the two decoupling heights is also plotted (dashed green).

Of the cases where the surface layer was thermodynamically decoupled from the cloud base, cases (b) and (e) had larger particle number concentrations within the surface layer, whereas cases (c), (d), and (f), had larger particle number concentrations above the lower boundary of the decoupling layer. The larger particle number concentrations near the surface during case (e) may have resulted from a build-up of local station pollution during an extended period of low wind speeds. Case (b) was the only day that was not impacted by precipitation either before or during sampling. The nucleation and scavenging of aerosol particles during precipitation events may have contributed to the depletion of aerosol particles in the isolated surface layers during cases (c), (d), and (f), and to the depleted layer just above the decoupling height during case (e). During case (f) there was intermittent light snow throughout the day, and on the other days, there were heavier snow events preceding the measurement period. Fog in the early morning of case (c), which is known to deplete surface aerosol particles at Summit (Bergin et al., 1994, 1995; Guy et al., 2021), could also have contributed to the reduced particle concentrations in the surface layer on this day.

For all the decoupled cases, the change in particle number concentrations and size distributions occurred 50 to 100 m above the lower boundary of the decoupling layer, suggesting that there is some entrainment mixing in the lowest part of the stable layer. Case (e) was unique in that a shallow layer that was depleted in aerosol particles occurred just above the lower boundary of the stable layer. Above the depleted layer particle number concentrations increased again to values similar to those at the

https://doi.org/10.5194/egusphere-2024-733
Preprint. Discussion started: 19 March 2024

onset of the stable layer (90 to 200 m, fig 4). This could suggest that the vertical profile of particle number concentration above the first inversion was consistent with height prior to modification by the precipitating cloud earlier in the day.

Applying the same methodology to detect below cloud decoupling layers to 932 radiosonde profiles from Summit during low-level clouds in June, July, and August 2010-2022 shows that the surface layer is decoupled from the sub-cloud layer 49% of the time (Shupe and Walden, 2010), which is similar to observations from the central Arctic Ocean (Sotiropoulou et al., 2014; Brooks et al., 2017; Vüllers et al., 2021). The average lowest decoupling height in this dataset was 120 m and 90% of decoupling heights were below 250 m. This implies that during half of the summer period over the central Greenland Ice Sheet, when surface melt is significantly influenced by cloud properties (e.g. Bennartz et al., 2013), surface aerosol measurements do not accurately represent the aerosol population relevant to cloud interactions. Consequently, relying solely on surface aerosol measurements is inadequate for studying cloud-aerosol interactions in this context. In winter months, surface aerosol measurements are even less likely to be representative of the cloud relevant population, since persistent high static stability at the surface occurs over 80% of the time (Miller et al., 2013), and clouds with base heights $< 2{,}000$ m are less common (Shupe et al., 2013). This could explain the particularly low surface aerosol particle number concentrations at Summit Station during the winter (Guy et al., 2021).

During this measurement campaign, we only sampled below-cloud vertical aerosol profiles. The above-cloud aerosol population can also be an important source of cloud-relevant aerosol particles in the Arctic (Igel et al., 2017) and can vary significantly from the below-cloud environment (Igel et al., 2017; Creamean et al., 2021; Lonardi et al., 2022). Future measurement campaigns should aim to characterise the vertical aerosol distribution below, within, and above the cloud environment over Greenland.

Lightweight aerosol particle sensors and robust and versatile measurement platforms are improving our ability to collect longer-term measurements of vertical aerosol profiles in remote places. However, the expensive resource cost of these in-situ measurements (most notably in terms of person-power) means that they will always be of limited duration. To fully characterise the cloud-relevant aerosol population over longer periods and in all seasons, focus should be placed on using in-situ measurements to develop, calibrate, and evaluate ground-based remote sensing instrumentation that can detect the vertical structure of aerosol particles near to the surface and that can operate unattended year-round. For example, high spectral resolution lidar can separate molecular scattering and aerosol particle scattering signals to retrieve vertical profiles of aerosol scattering properties (e.g. Thorsen and Fu, 2015; Zhang et al., 2022). However, the relationship between aerosol scattering properties and cloud-relevant aerosol properties (i.e. particle size distribution or CCN concentration) varies depending on aerosol composition and shape (e.g. Ghan and Collins, 2004; Lv et al., 2018; Tan et al., 2019), and retrieving aerosol vertical profiles in the vicinity of clouds is complicated by precipitation and hygroscopic growth (e.g. Schmidt et al., 2014). Since lidar cannot detect aerosol particles through optically thick cloud, in-situ measurements remain the only way to sample the above cloud vertical aerosol profile.

https://doi.org/10.5194/egusphere-2024-733
Preprint. Discussion started: 19 March 2024

5 Summary and conclusions

This report presents the first in-situ measurements of below-cloud vertically resolved aerosol particle size distributions over the central Greenland Ice Sheet. Although this campaign was limited to just nine vertical profiles on six opportunistic sampling days, the measurements demonstrate that surface-based aerosol measurements are not always representative of the cloud-relevant aerosol population over central Greenland. Thermodynamic decoupling between the surface and the cloud layer occurred on five of the six sampling days below horizontally extensive low-level cloud (cloud base 315 to 1,680 m), and distinct variations in the aerosol particle size distribution with height were associated with the decoupling layers in each case. The fact that thermodynamic decoupling of the surface from cloud layers with bases $< 2{,}000$ m occurs 49% of the time during the summer in central Greenland suggests that surface aerosol measurements are insufficient to describe the cloud-relevant aerosol population half of the time. Given that the presence and LWP of low-level clouds are an important control on the ice sheet surface energy budget, and that the aerosol population can potentially modulate cloud LWP and lifetime, a concerted effort to understand aerosol vertical profiles and their importance for cloud-aerosol interactions over the Greenland Ice Sheet is warranted.

This measurement campaign demonstrates that a tethered balloon system carrying a simple optical particle counter can collect novel data about the vertical structure of the aerosol population in the lowest 800 m above the surface in extreme conditions (freezing temperatures and low pressures) over the central Greenland Ice Sheet. Future campaigns should aim to sample both below and above cloud layers and should focus on characterising intra- and inter-seasonal variability and combining in-situ measurements with automated ground-based remote sensing to work towards the possibility of long-term measurements.

Data availability. All data collected during this measurement campaign will be publicly available at the CEDA data archive, preliminary data can be accessed at: https://gws-access.jasmin.ac.uk/public/icecaps/Helikite2023/ (Guy et al., 2024). Complementary data from the ICECAPS project are available at the Arctic Data Center, at doi:10.18739/A20C4SM02 (ceilometer) and doi:10.18739/A2445HD3Q (radiosondes).

Author contributions. RN and HG conceptualised and planned the measurement campaign. AM, EO, and HG carried out the measurements in Greenland with offsite supervision from RN. HG led the data curation, analysis and visualisation with contributions from all co-authors. IB contributed to the analysis of the Windsonde data and boundary layer structure. HG wrote the manuscript with feedback from all co-authors.

Competing interests. The authors declare that they have no conflict of interest.

https://doi.org/10.5194/egusphere-2024-733
Preprint. Discussion started: 19 March 2024

Acknowledgements. Thank you to staff and personnel at Summit Station during summer 2023 for exceptional support during the field campaign, and to Polar Field services for organisation and coordination of fieldwork activities. We are grateful to the Danish Civil Aviation Authority and Nuuk Flight Information Services for permission to fly the tethered balloon in the Northeast Greenland National Park. We acknowledge financial support from NSFGEO-NERC grants NE/X002403/1 and NE/S00906X/1. AM was also supported by the NERC SENSE-CDT NE/T00939X/1.

https://doi.org/10.5194/egusphere-2024-733
Preprint. Discussion started: 19 March 2024

References

Allsopp Helikites Ltd.: http://www.allsopp.co.uk/, accessed: 2023-12-11, 2023.

Bennartz, R., Shupe, M. D., Turner, D. D., Walden, V., Steffen, K., Cox, C. J., Kulie, M. S., Miller, N. B., and Pettersen, C.: July 2012 Greenland melt extent enhanced by low-level liquid clouds, Nature, 496, 83–86, 2013.

Bergin, M., Jaffrezo, J., Davidson, C., Caldow, R., and Dibb, J.: Fluxes of chemical species to the Greenland ice sheet at Summit by fog and dry deposition, Geochimica et cosmochimica acta, 58, 3207–3215, 1994.

Bergin, M., Jaffrezo, J.-L., Davidson, C., Dibb, J. E., Pandis, S., Hillamo, R., Maenhaut, W., Kuhns, H., and Makela, T.: The contributions of snow, fog, and dry deposition to the summer flux of anions and cations at Summit, Greenland, Journal of Geophysical Research: Atmospheres, 100, 16 275–16 288, 1995.

Brooks, I. M., Tjernström, M., Persson, P. O. G., Shupe, M. D., Atkinson, R. A., Canut, G., Birch, C. E., Mauritsen, T., Sedlar, J., and Brooks, B. J.: The turbulent structure of the Arctic summer boundary layer during the Arctic summer cloud-ocean study, Journal of Geophysical Research: Atmospheres, 122, 9685–9704, 2017.

Creamean, J. M., de Boer, G., Telg, H., Mei, F., Dexheimer, D., Shupe, M. D., Solomon, A., and McComiskey, A.: Assessing the vertical structure of Arctic aerosols using balloon-borne measurements, Atmospheric Chemistry and Physics, 21, 1737–1757, 2021.

Dibb, J. E., Jaffrezo, J., and Legrand, M.: Initial findings of recent investigations of air-snow relationships in the Summit region of the Greenland Ice Sheet, Journal of Atmospheric Chemistry, 14, 167–180, 1992.

Flyger, H., Hansen, K., Megaw, W., and Cox, L.: The background level of the summer tropospheric aerosol over Greenland and the North Atlantic Ocean, Journal of Applied Meteorology and Climatology, 12, 161–174, 1973.

Flyger, H., Heidam, N., Hansen, K., Megaw, W., Walther, E., and Hogan, A.: The background level of the summer tropospheric aerosol, sulphur dioxide and ozone over Greenland and the North Atlantic Ocean, Journal of Aerosol Science, 7, 103–140, 1976.

Freud, E., Krejci, R., Tunved, P., Leaitch, R., Nguyen, Q. T., Massling, A., Skov, H., and Barrie, L.: Pan-Arctic aerosol number size distributions: Seasonality and transport patterns, Atmospheric Chemistry and Physics, 17, 8101–8128, 2017.

Gao, R., Telg, H., McLaughlin, R., Ciciora, S., Watts, L., Richardson, M., Schwarz, J., Perring, A., Thornberry, T., Rollins, A., et al.: A light-weight, high-sensitivity particle spectrometer for PM2.5 aerosol measurements, Aerosol Science and Technology, 50, 88–99, 2016.

Ghan, S. J. and Collins, D. R.: Use of in situ data to test a Raman lidar–based cloud condensation nuclei remote sensing method, Journal of Atmospheric and Oceanic Technology, 21, 387–394, 2004.

Guy, H., Brooks, I. M., Carslaw, K. S., Murray, B. J., Walden, V. P., Shupe, M. D., Pettersen, C., Turner, D. D., Cox, C. J., Neff, W. D., et al.: Controls on surface aerosol particle number concentrations and aerosol-limited cloud regimes over the central Greenland Ice Sheet, Atmospheric Chemistry and Physics, 21, 15 351–15 374, 2021.

Guy, H., Brooks, I. M., Turner, D. D., Cox, C. J., Rowe, P. M., Shupe, M. D., Walden, V. P., and Neely III, R. R.: Observations of fog-aerosol interactions over central Greenland, Journal of Geophysical Research: Atmospheres, p. e2023JD038718, 2023.

Guy, H., Brooks, I. M., and Neely III, R. R.: Vertical aerosol particle size distributions and radiosonde measurements collected at Summit Station, Greenland, July-August 2023 [Preliminary data set], https://gws-access.jasmin.ac.uk/public/icecaps/Helikite2023/, 2024.

Hirdman, D., Sodemann, H., Eckhardt, S., Burkhart, J. F., Jefferson, A., Mefford, T., Quinn, P. K., Sharma, S., Ström, J., and Stohl, A.: Source identification of short-lived air pollutants in the Arctic using statistical analysis of measurement data and particle dispersion model output, Atmospheric Chemistry and Physics, 10, 669–693, 2010.

https://doi.org/10.5194/egusphere-2024-733
Preprint. Discussion started: 19 March 2024

Hoch, S., Calanca, P., Philipona, R., and Ohmura, A.: Year-round observation of longwave radiative flux divergence in Greenland, Journal of Applied Meteorology and Climatology, 46, 1469–1479, 2007.

Hofer, S., Tedstone, A. J., Fettweis, X., and Bamber, J. L.: Decreasing cloud cover drives the recent mass loss on the Greenland Ice Sheet, Science Advances, 3, e1700 584, 2017.

Howat, I., Negrete, A., and Smith, B.: The Greenland Ice Mapping Project (GIMP) Land Ice and Ocean Classification Mask, Version 1., NASA National Snow and Ice Data Center Distributed Active Archive Center., https://doi.org/https://doi.org/10.5067/B8X58MQBFUPA, 2017.

Igel, A. L., Ekman, A. M., Leck, C., Tjernström, M., Savre, J., and Sedlar, J.: The free troposphere as a potential source of arctic boundary layer aerosol particles, Geophysical Research Letters, 44, 7053–7060, 2017.

Korolev, A.: Limitations of the Wegener–Bergeron–Findeisen mechanism in the evolution of mixed-phase clouds, Journal of the Atmospheric Sciences, 64, 3372–3375, 2007.

Lange, R., Dall'Osto, M., Skov, H., Nøjgaard, J., Nielsen, I., Beddows, D., Simó, R., Harrison, R. M., and Massling, A.: Characterization of distinct Arctic aerosol accumulation modes and their sources, Atmospheric Environment, 183, 1–10, 2018.

Law, K. S., Stohl, A., Quinn, P. K., Brock, C. A., Burkhart, J. F., Paris, J.-D., Ancellet, G., Singh, H. B., Roiger, A., Schlager, H., et al.: Arctic air pollution: New insights from POLARCAT-IPY, Bulletin of the American Meteorological Society, 95, 1873–1895, 2014.

Lonardi, M., Pilz, C., Akansu, E. F., Dahlke, S., Egerer, U., Ehrlich, A., Griesche, H., Heymsfield, A. J., Kirbus, B., Schmitt, C. G., et al.: Tethered balloon-borne profile measurements of atmospheric properties in the cloudy atmospheric boundary layer over the Arctic sea ice during MOSAiC: Overview and first results, Elem Sci Anth, 10, 000 120, 2022.

Lv, M., Wang, Z., Li, Z., Luo, T., Ferrare, R., Liu, D., Wu, D., Mao, J., Wan, B., Zhang, F., et al.: Retrieval of cloud condensation nuclei number concentration profiles from lidar extinction and backscatter data, Journal of Geophysical Research: Atmospheres, 123, 6082–6098, 2018.

Mauritsen, T., Sedlar, J., Tjernström, M., Leck, C., Martin, M., Shupe, M., Sjogren, S., Sierau, B., Persson, P., Brooks, I., et al.: An Arctic CCN-limited cloud-aerosol regime, Atmospheric Chemistry and Physics, 11, 165–173, 2011.

Mei, F., McMeeking, G., Pekour, M., Gao, R.-S., Kulkarni, G., China, S., Telg, H., Dexheimer, D., Tomlinson, J., and Schmid, B.: Performance Assessment of Portable Optical Particle Spectrometer (POPS), Sensors, 20, https://doi.org/10.3390/s20216294, 2020.

Miller, N., Turner, D., Bennartz, R., Shupe, M., Kulie, M., Cadeddu, M., and Walden, V. P.: Surface-based inversions above central Greenland, Journal of Geophysical Research: Atmospheres, 118, 495–506, 2013.

Miller, N. B., Shupe, M. D., Cox, C. J., Walden, V. P., Turner, D. D., and Steffen, K.: Cloud radiative forcing at Summit, Greenland, Journal of Climate, 28, 6267–6280, 2015.

Münkel, C., Eresmaa, N., Räsänen, J., and Karppinen, A.: Retrieval of mixing height and dust concentration with lidar ceilometer, Boundary-layer meteorology, 124, 117–128, 2007.

Nguyen, Q. T., Glasius, M., Sørensen, L. L., Jensen, B., Skov, H., Birmili, W., Wiedensohler, A., Kristensson, A., Nøjgaard, J. K., and Massling, A.: Seasonal variation of atmospheric particle number concentrations, new particle formation and atmospheric oxidation capacity at the high Arctic site Villum Research Station, Station Nord, Atmospheric Chemistry and Physics, 16, 11 319–11 336, 2016.

NOAA-GML: Meteorology Measurements from the NOAA/ESRL/GMD Baseline Observatory Summit Station, NOAA-GML [data set], https://gml.noaa.gov/aftp/data/meteorology/in-situ/sum/2023, last accessed: 15 December 2023, 2023.

https://doi.org/10.5194/egusphere-2024-733
Preprint. Discussion started: 19 March 2024

Schmale, J., Sharma, S., Decesari, S., Pernov, J., Massling, A., Hansson, H.-C., Von Salzen, K., Skov, H., Andrews, E., Quinn, P. K., et al.: Pan-Arctic seasonal cycles and long-term trends of aerosol properties from ten observatories, Atmospheric Chemistry and Physics Discussions, 2021, 1–53, 2021.

Schmidt, J., Ansmann, A., Bühl, J., Baars, H., Wandinger, U., Mueller, D., and Malinka, A. V.: Dual-FOV Raman and Doppler lidar studies of aerosol-cloud interactions: Simultaneous profiling of aerosols, warm-cloud properties, and vertical wind, Journal of Geophysical Research: Atmospheres, 119, 5512–5527, 2014.

Shupe, M. D. and Intrieri, J. M.: Cloud radiative forcing of the Arctic surface: The influence of cloud properties, surface albedo, and solar zenith angle, Journal of climate, 17, 616–628, 2004.

Shupe, M. D. and Walden, V. P.: Radiosonde temperature and humidity profiles taken at Summit Station, Greenland [data set], https://doi.org/10.18739/A2445HD3Q, 2010.

Shupe, M. D., Turner, D. D., Walden, V. P., Bennartz, R., Cadeddu, M. P., Castellani, B. B., Cox, C. J., Hudak, D. R., Kulie, M. S., Miller, N. B., et al.: High and dry: New observations of tropospheric and cloud properties above the Greenland Ice Sheet, Bulletin of the American Meteorological Society, 94, 169–186, 2013.

Sotiropoulou, G., Sedlar, J., Tjernström, M., Shupe, M. D., Brooks, I. M., and Persson, P. O. G.: The thermodynamic structure of summer Arctic stratocumulus and the dynamic coupling to the surface, Atmospheric Chemistry and Physics, 14, 12 573–12 592, 2014.

Sterzinger, L. J., Sedlar, J., Guy, H., Neely III, R. R., and Igel, A. L.: Do Arctic mixed-phase clouds sometimes dissipate due to insufficient aerosol? Evidence from comparisons between observations and idealized simulations, Atmospheric Chemistry and Physics, 22, 8973–8988, 2022.

Storelvmo, T., Hoose, C., and Eriksson, P.: Global modeling of mixed-phase clouds: The albedo and lifetime effects of aerosols, Journal of Geophysical Research: Atmospheres, 116, 2011.

Tan, W., Zhao, G., Yu, Y., Li, C., Li, J., Kang, L., Zhu, T., and Zhao, C.: Method to retrieve cloud condensation nuclei number concentrations using lidar measurements, Atmospheric Measurement Techniques, 12, 3825–3839, 2019.

Thorsen, T. J. and Fu, Q.: Automated retrieval of cloud and aerosol properties from the ARM Raman lidar. Part II: Extinction, Journal of Atmospheric and Oceanic Technology, 32, 1999–2023, 2015.

Twomey, S.: The influence of pollution on the shortwave albedo of clouds, Journal of the atmospheric sciences, 34, 1149–1152, 1977.

Van Tricht, K., Lhermitte, S., Lenaerts, J. T., Gorodetskaya, I. V., L'Ecuyer, T. S., Noël, B., van den Broeke, M. R., Turner, D. D., and van Lipzig, N. M.: Clouds enhance Greenland ice sheet meltwater runoff, Nature communications, 7, 10 266, 2016.

Vüllers, J., Achtert, P., Brooks, I. M., Tjernström, M., Prytherch, J., Burzik, A., and Neely III, R.: Meteorological and cloud conditions during the Arctic Ocean 2018 expedition, Atmospheric Chemistry and Physics, 21, 289–314, 2021.

Zhang, D., Comstock, J., Xie, H., and Wang, Z.: Polar Aerosol Vertical Structures and Characteristics Observed with a High Spectral Resolution Lidar at the ARM NSA Observatory, Remote Sensing, 14, 4638, 2022.